

University of Groningen

Unchaining miniBacillus PG10

van Tilburg, Amanda Y; Fülleborn, Julius A; Reder, Alexander; Völker, Uwe; Stülke, Jörg; van Heel, Auke J; Kuipers, Oscar P

Published in:
Applied and environmental microbiology

DOI:
[10.1128/AEM.01123-21](https://doi.org/10.1128/AEM.01123-21)

IMPORTANT NOTE: You are advised to consult the publisher's version (publisher's PDF) if you wish to cite from it. Please check the document version below.

Document Version
Publisher's PDF, also known as Version of record

Publication date:
2021

[Link to publication in University of Groningen/UMCG research database](#)

Citation for published version (APA):

van Tilburg, A. Y., Fülleborn, J. A., Reder, A., Völker, U., Stülke, J., van Heel, A. J., & Kuipers, O. P. (2021). Unchaining miniBacillus PG10: Relief of FlgM-mediated repression of autolysin genes. *Applied and environmental microbiology*, 87(18), [e01123-21]. <https://doi.org/10.1128/AEM.01123-21>

Copyright

Other than for strictly personal use, it is not permitted to download or to forward/distribute the text or part of it without the consent of the author(s) and/or copyright holder(s), unless the work is under an open content license (like Creative Commons).

The publication may also be distributed here under the terms of Article 25fa of the Dutch Copyright Act, indicated by the "Taverne" license. More information can be found on the University of Groningen website: <https://www.rug.nl/library/open-access/self-archiving-pure/taverne-amendment>.


Take-down policy

If you believe that this document breaches copyright please contact us providing details, and we will remove access to the work immediately and investigate your claim.

Downloaded from the University of Groningen/UMCG research database (Pure): <http://www.rug.nl/research/portal>. For technical reasons the number of authors shown on this cover page is limited to 10 maximum.



Unchaining mini*Bacillus* Strain PG10: Relief of FlgM-Mediated Repression of Autolysin Genes

Amanda Y. van Tilburg,^a Julius A. Fülleborn,^a Alexander Reder,^b Uwe Völker,^b Jörg Stülke,^c Auke J. van Heel,^a  Oscar P. Kuipers^a

^aDepartment of Molecular Genetics, University of Groningen, Groningen, the Netherlands

^bInterfaculty Institute for Genetics and Functional Genomics, University Medicine Greifswald, Greifswald, Germany

^cInstitute of Microbiology and Genetics, Georg-August University Göttingen, Göttingen, Germany

ABSTRACT Cell chaining in *Bacillus subtilis* is naturally observed in a subset of cells during exponential growth and during biofilm formation. However, the recently constructed large-scale genome-minimized *B. subtilis* strain PG10 displays a severe and permanent defect in cell separation, as it exclusively grows in the form of long filaments of nonseparated cells. In this study, we investigated the underlying mechanisms responsible for the incomplete cell division of PG10 by genomic and transcriptomic analyses. Repression of the SigD regulon, including the major autolysin gene *lytF*, was identified as the cause for the cell separation problem of PG10. It appeared that SigD-regulated genes are downregulated in PG10 due to the absence of the flagellar export apparatus, which normally is responsible for secretion of FlgM, the anti-sigma factor of SigD. Although mild negative effects on growth and cell morphology were observed, deletion of *flgM* could revert the aberrant cell-chaining phenotype and increased transformation efficiency. Interestingly, our work also demonstrates the occurrence of increased antisense transcription of *slrR*, a transcriptional repressor of autolysin genes, in PG10 and provides further understanding for this observation. In addition to revealing the molecular basis of the cell separation defect in PG10, our work provides novel targets for subsequent genome reduction efforts and future directions for further optimization of mini*Bacillus* PG10.

IMPORTANCE Reduction of the size of bacterial genomes is relevant for understanding the minimal requirements for cellular life as well as from a biotechnological point of view. Although the genome-minimized *Bacillus subtilis* strain PG10 displays several beneficial traits as a microbial cell factory compared to its parental strain, a defect at the final stage of cell division was introduced during the genome reduction process. By genetic and transcriptomic analyses, we identified the underlying reasons for the cell separation problem of PG10. In addition to enabling PG10 to grow in a way similar to that of *B. subtilis* wild-type strains, our work points toward subsequent targets for fine-tuning and further reduction of the genome of PG10. Moreover, solving the cell separation defect facilitates laboratory handling of PG10 by increasing the transformation efficiency, among other means. Overall, our work contributes to understanding and improving biotechnologically attractive minimal bacterial cell factories.

KEYWORDS mini*Bacillus*, genome minimization, daughter cell separation, autolysins, sigma factor D, cell separation

Reconstruction and minimization of bacterial genomes contributes to understanding the minimal requirements for cellular life. For the model organism *Bacillus subtilis*, a milestone in genome reduction was achieved by the construction and characterization of two independent mini*Bacillus* strains with a reduction of ~36% in genome size compared to the original parental strain, *B. subtilis* 168 (1). These strains, named PG10 and PS38, resulted from the stepwise, markerless deletion of dispensable genomic regions

Citation van Tilburg AY, Fülleborn JA, Reder A, Völker U, Stülke J, van Heel AJ, Kuipers OP. 2021. Unchaining mini*Bacillus* strain PG10: relief of FlgM-mediated repression of autolysin genes. *Appl Environ Microbiol* 87:e01123-21. <https://doi.org/10.1128/AEM.01123-21>.

Editor Maia Kivisaar, University of Tartu

Copyright © 2021 American Society for Microbiology. All Rights Reserved.

Address correspondence to Oscar P. Kuipers, o.p.kuipers@rug.nl.

Received 7 June 2021

Accepted 23 June 2021

Accepted manuscript posted online 7 July 2021

Published 26 August 2021

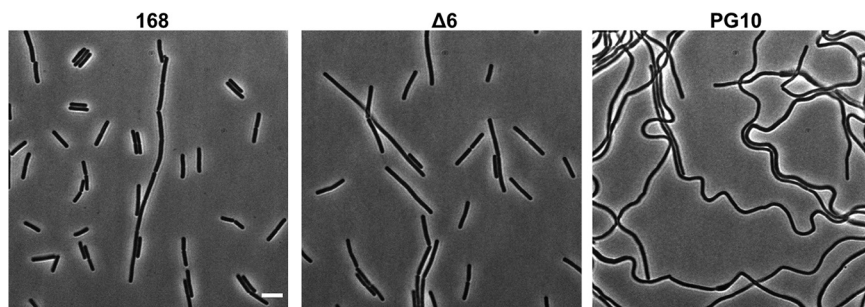


FIG 1 *miniBacillus* PG10 grows as long filaments of chained cells compared to its progenitor strains, *B. subtilis* 168 and $\Delta 6$. Phase-contrast microscopy images of cells grown to mid-exponential phase. Scale bar represents 5 μm .

starting from the previously constructed *B. subtilis* $\Delta 6$ strain, whose genome was already reduced by 7.7% (2). In addition to defining a minimal set of genes necessary for cellular life, these large-scale genome-minimized strains are attractive minimal cell factories for biotechnological applications. Two different studies demonstrated several advantages of *miniBacillus* PG10 for the heterologous production of peptides or proteins compared to their production in *B. subtilis* 168 or the protease-deficient strain WB800 (3, 4). The successful performance of PG10 as a heterologous production host was attributed to reduced proteolytic activity, a cleaner metabolic background, and enhanced translational activity.

Interest in *miniBacillus* PG10 and PS38 as attractive heterologous expression hosts is also related to the fact that they are still easy to genetically engineer due to the conservation of the commonly used integration loci *amyE* and *thrC* as well as to their ability to become genetically competent (1). Moreover, the strains display robust growth in complex medium (LB), with only a slight decrease in growth rate compared to the $\Delta 6$ reference strain. However, one striking phenotypic abnormality is clearly visible for PG10 and PS38: they grow in the form of long filaments of non-separated cells (Fig. 1). Therefore, the strains seem to display a defect in the final stage of cell division. Thus, this presents a target for further optimization of the *miniBacillus* strains, which at least might ease laboratory handling of the strains, as no firm cell pellets can be obtained after centrifugation (see Fig. 5C). Possibly, resolving the cell separation problem of the *miniBacillus* strains might also impact their productivity as a minimal cell factory.

At the end of cell division, daughter cells are separated from each other by autolysins that cleave the peptidoglycan across the long axis of the division septum (5). Although the genome of *B. subtilis* encodes at least 35 different autolysins, LytF has been identified as the primary autolysin responsible for daughter cell separation (6). In *B. subtilis*, chaining of cells can be observed during biofilm formation as well as during mid-exponential growth, where a mixed population of individual motile cells and chains of sessile cells coexists (7, 8). Transcription of autolysin genes and motility genes requires the alternative sigma factor D (SigD) to be bound to RNA polymerase (9–13). In agreement with this, a *sigD* mutant strain forms long chains of cells, and daughter cell separation can be restored by inducible expression of *lytF* (6). The activity of SigD is controlled by its anti-sigma factor, FlgM, whose intracellular level in turn is regulated by the assembly of the flagellar secretion apparatus (14). The majority of genes encoding the flagellar secretion apparatus are located in the *fla-che* operon, which also encodes *sigD* (15, 16). In the initial stage of flagellar assembly, the activity of SigD is inhibited by binding to its anti-sigma factor, FlgM (17–19). Upon completion of the flagellar hook-basal body, FlgM is secreted into the extracellular space, thereby liberating SigD and enabling transcription of the SigD regulon (14). Another level of regulation of daughter cell separation is governed by the SlrR•SinR bistable switch (20). SinR and SlrR form a double-negative feedback loop, which can exist in an SlrR^{HIGH} or SlrR^{LOW} state. In an SlrR^{LOW} state, matrix genes and *slrR* are repressed by SinR, enabling cells to

TABLE 1 Differential expression levels of genes associated with cell separation in mini*Bacillus* PG10^a

Locus	Gene name	Function	Fold change	P value
BSU35430	<i>flgM</i>	Anti-sigma factor of SigD	2.1	7.65E-03
BSU35640	<i>lytA</i>	Secretion of LytC	-5.4	5.85E-06
BSU35630	<i>lytB</i>	Modifier protein of LytC	-5.2	5.04E-06
BSU35620	<i>lytC</i>	N-Acetylmuramoyl-L-alanine amidase, autolysin, required for flagellar function	-4.8	5.45E-06
BSU09370	<i>lytF</i>	Gamma-D-glutamate-meso-diaminopimelate muropeptidase, major autolysin	-6.7	1.19E-05

^aTiling microarray data (1) were compared between PG10 and the reference strain Δ6. Only genes with a fold change of >2 are shown.

grow as individual and motile cells. In contrast, cells that are in an SlrR^{HIGH} state are chaining and immobile because of SlrR-mediated repression of autolysin and motility genes. Either due to deterministic induction (biofilm formation) or stochastic expression (exponential growth) of *sinI*, cells can switch from an SlrR^{LOW} to an SlrR^{HIGH} state (7, 20, 21).

Although cell chaining occurs naturally under the conditions described above, PG10 clearly has a severe and permanent defect in cell separation, which might limit its full potential as a minimal cell factory. Therefore, the main goal of this study was to investigate the underlying mechanism(s) responsible for the cell separation defect in mini*Bacillus* PG10. For that purpose, we analyzed the differences at the genomic and transcriptomic levels between PG10 and its progenitor Δ6 strain, which does not display a severe cell chaining phenotype. Repression of the SigD regulon, which also contains the major autolysin-encoding gene, *lytF*, was identified as the underlying reason for the cell separation defect of PG10. The activity of SigD appeared to be inhibited by intracellular accumulation of its anti-sigma factor FlgM due to the absence of the flagellar export apparatus in PG10 (as a consequence of genome reduction). By resolving the cell separation problem of PG10, the transformation efficiency increased by about 10-fold, and laboratory handling of this mini*Bacillus* strain became more convenient. In addition, novel directions for subsequent genome reduction steps could be identified.

RESULTS

Transcriptome analysis reveals downregulation of autolysin genes in PG10. To investigate whether the large-scale genome reduction had caused deregulation of genes involved in cell separation in PG10, a transcriptomic comparison between PG10 and its progenitor strain, Δ6, was performed. For this purpose, tiling array data derived from the initial characterization of PG10 (1) was analyzed using the GEO2R software.

Five genes involved in cell separation showed a significant differential expression in PG10 compared to Δ6 (Table 1). Interestingly, an ~5- to 7-fold downregulation of the *lytABC* operon and the major autolysin gene *lytF* was observed in PG10. In addition, the expression level of *flgM*, the anti-sigma factor of SigD, was ~2-fold increased. Other effectors that are also involved in cell separation but remained unaffected in PG10 included the alternative sigma factor SigD, the transcriptional regulators SlrR and SinR, and the SinR antagonists SinI and SlrA. It is worth noting that although the average number of sense transcripts of *slrR* was comparable between PG10 and Δ6, antisense transcription of *slrR* was nearly 8-fold increased in PG10 (see Table S1 in the supplemental material). The above-described findings suggest that the aberrant chaining phenotype of PG10 is caused by downregulation of autolysin genes. The SlrR•SinR bistable switch does not seem to be responsible for the repression of autolysin genes, since *slrR* rather seems to be silenced in PG10 due to the increased level of antisense transcripts. In agreement with this, extensive cell chaining was still observed upon deletion of *slrR* in PG10 (Fig. S1). Therefore, it was concluded that compromised activity of SigD, e.g., by upregulation of *flgM*, is responsible for the observed downregulation of autolysin genes in PG10.

Inducible expression of the major autolysin gene *lytF* resolves cell chaining in PG10. In *B. subtilis*, LytF has been identified as a major autolysin, since inducible expression of *lytF* could revert cell chaining in a *sigD* mutant strain (6). To investigate whether the observed downregulation of autolysin genes led to the cell separation

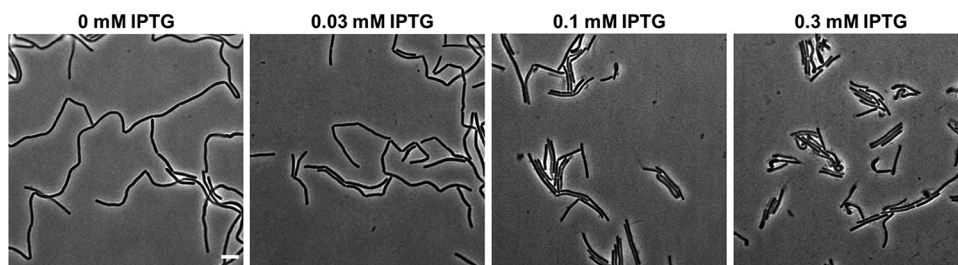


FIG 2 Inducible expression of *lytF* reverts extensive cell chaining in PG10. Phase-contrast microscopy was performed of PG10 containing an IPTG-inducible copy of *lytF* (controlled by the hyperspank promoter; $P_{spank-hy}$). Cultures were grown to mid-exponential phase in LB containing various concentrations of IPTG as indicated. Scale bar represents 5 μm .

defect in PG10, an isopropyl- β -D-thiogalactopyranoside (IPTG)-inducible copy of *lytF* was introduced in the *amyE* locus of PG10. As visualized in Fig. 2, the cell chaining phenotype of PG10 could be resolved upon artificial expression of *lytF*. Notably, with increasing concentrations of IPTG, extrusions at cell poles and aggregation of cells could be observed. Nevertheless, these results provide a good indication that the extensive cell chaining of PG10 cells is a consequence of downregulation of autolysin genes.

Downregulation of the SigD regulon in PG10. As mentioned earlier, the alternative sigma factor SigD is an important player in daughter cell separation in *B. subtilis*. Importantly, *sigD* mutants display an extensive cell chaining phenotype like PG10 (7, 9), and transcription of *lytF* is fully dependent on binding of SigD to RNA polymerase (22). Although no differences were observed on the mRNA or protein level of *sigD*/SigD (Table 1 and reference 1), we hypothesized that altered SigD activity leads to the chaining phenotype of PG10. To substantiate this hypothesis, expression levels of genes that are exclusively under the control of SigD as a sigma factor (and still present in PG10) were analyzed. Interestingly, significantly affected SigD-regulated genes were all downregulated in PG10 compared to the $\Delta 6$ reference strain (Table 2). The four genes showing the most drastic decrease in gene expression were the major autolysin gene *lytF*, the chemotaxis receptor genes *hemAT* and *yfmS*, and *yjcM*, encoding a protein of unknown function. The finding that other SigD-regulated genes, in addition to *lytF*, are downregulated in PG10 suggests that compromised SigD activity is responsible for cell chaining in PG10.

Intracellular accumulation of FlgM, the anti-sigma factor of SigD, is responsible for the permanent repression of autolysin genes in PG10. In *B. subtilis*, expression of SigD-regulated genes is coupled to the assembly of the flagellar export apparatus. This represents a kind of checkpoint that combines completion of the flagellar hook-basal

TABLE 2 Differential expression levels of SigD-dependent genes^a

Locus	Gene name	Function	Fold change	P value
BSU03440	<i>tlpC</i>	Chemotaxis receptor	-2.4	6.35E-03
BSU07360	<i>yfmS</i>	Chemotaxis receptor	-9.1	2.85E-06
BSU09370	<i>lytF</i>	Major autolysin	-6.7	1.19E-05
BSU10380	<i>hemAT</i>	Chemotaxis receptor	-14.6	2.19E-06
BSU11910	<i>yjcM</i>	Unknown	-6.2	1.06E-04
BSU13420	<i>dgcW</i>	Synthesis of c-di-GMP	-5.1	2.40E-04
BSU15960	<i>ylqB</i>	Control of entry into sporulation	-1.6	4.45E-02
BSU21940	<i>degR</i>	Control of DegU activity	-1.7	2.32E-02
BSU28890	<i>yscB</i>	Unknown	-2.1	3.53E-02
BSU33690	<i>yvaQ</i>	Chemotaxis receptor	-2.0	2.47E-03
BSU33870	<i>yvbl</i>	Unknown	-2.3	1.46E-03
BSU36390	<i>flhP</i>	Flagellar hook-basal-body rod protein	-1.8	1.31E-02
BSU36400	<i>flhO</i>	Flagellar basal-body rod protein	-1.8	1.38E-02

^aTiling microarray data (1) were compared between PG10 and the reference strain $\Delta 6$. Only genes that are exclusively dependent on SigD for their transcription and with an adjusted P value of ≤ 0.05 are shown.

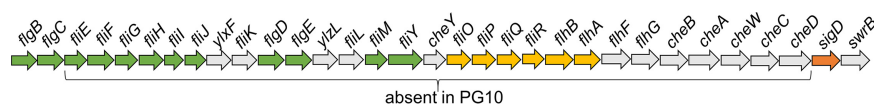


FIG 3 Schematic representation of the *fla-che* operon in *B. subtilis*. Genes visualized in green encode flagellar structural components, and genes visualized in yellow encode proteins of the type II export apparatus. *sigD* is colored in orange. Note that the majority of genes of the *fla-che* operon have been deleted in PG10.

body assembly with SigD activity control by secretion of FlgM, the anti-sigma factor of SigD (14). The *fla-che* operon (Fig. 3) contains most of the genes encoding the individual proteins of the flagellar export apparatus (15, 16). However, in mini*Bacillus* PG10, the majority of genes of the *fla-che* operon are absent (from *flgE* until and including *cheD*) as a consequence of the deletion of genomic regions unnecessary for survival (1). In contrast, *flgM* was preserved during the genome reduction process. Thus, in addition to the 2-fold upregulation of *flgM*, secretion of FlgM is likely abolished in PG10, resulting in permanent accumulation of FlgM and repression of SigD-regulated genes. To test this hypothesis, *flgM* was deleted in PG10. Microscopic analysis revealed that the *flgM* deletion strain mainly grew in the form of separate cells (Fig. 4). This indicates that cell separation autolysin genes cannot be transcribed in PG10 due to the permanent inhibition of SigD activity by intracellularly accumulated FlgM.

Consequences of unchaining PG10 by deletion of *flgM*. Similar to PG10 cells in which *lytF* expression was induced, cellular aggregates and polar extrusions could be observed for the *flgM* deletion strain to a limited extent (Fig. 4). Moreover, unchaining PG10, either via deletion of *flgM* or by induction of *lytF*, impaired cell growth (Fig. 5A and Table S2). This was clearly visible later in the growth phase, resulting in a decreased final optical density for the PG10 mutant strains (maximum optical density at 600 nm [OD₆₀₀] of 1.8 compared to a final OD₆₀₀ of 3.0 for the PG10 wild type). Statistical analysis indicated that deletion of *flgM* or induction of *lytF* significantly affected the growth of PG10 after at least 4 h of growth. However, positive consequences of resolving the cell chaining problem of PG10 also were noted. Upon deletion of *flgM*, the transformation efficiency significantly increased by almost 1 order of magnitude compared to the PG10 wild type (Fig. 5B). In addition, *flgM* deletion strains formed more firm cell pellets (Fig. 5C), thereby making the handling of unchained PG10 cells easier and less time-consuming.

DISCUSSION

As a starting point for the successive genome reduction of *B. subtilis*, a minimal set of genes was defined based on certain criteria (23). This selection process was facilitated by the vast amount of information available regarding genome annotation, essential genes, and cellular processes in *B. subtilis*. One of these criteria was that the growth and physiology of the genome-minimized strains in complex medium should

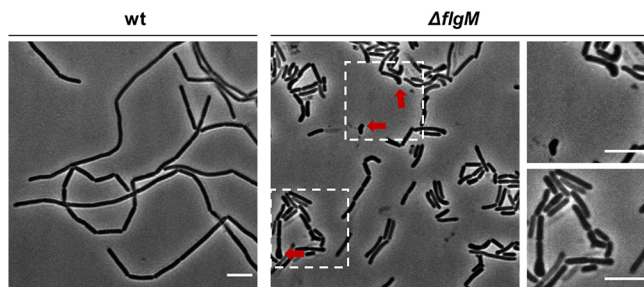


FIG 4 Deletion of *flgM* enables PG10 to grow as separate cells. Phase-contrast microscopy pictures were taken in the exponential growth phase of PG10 wild type and PG10 Δ *flgM* mutant. Arrows indicate examples of cellular extrusions/abnormalities of which zoomed images (white boxes) are shown on the right. Scale bars represent 5 μ m.

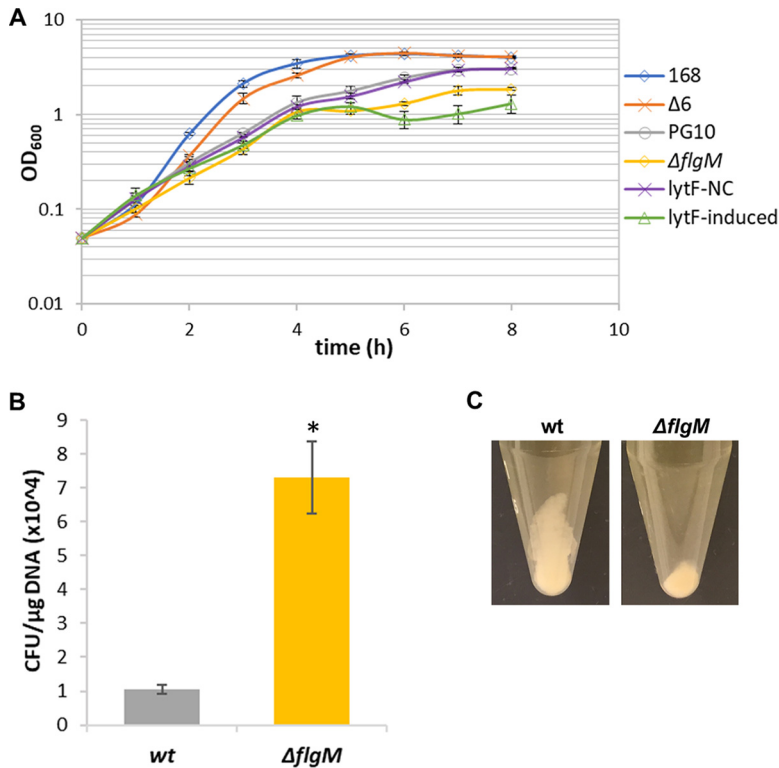


FIG 5 Consequences of unchaining PG10 on its growth and laboratory use. (A) Effect of deletion of *flgM* or IPTG-inducible *lytF* expression on the growth of PG10. Average OD₆₀₀ values and standard deviations were determined from triplicate OD₆₀₀ measurements. lytF-NC and lytF-induced correspond to PG10 *lytF* grown without induction and with induction (0.03 mM IPTG) of *lytF*, respectively. Growth curves of the progenitor strains of PG10, *B. subtilis* 168 and *B. subtilis* Δ6, are also shown. *P* values of pairwise comparison between PG10 wild-type and mutant strains at each time point can be found in Table S2. (B) Transformation efficiency of PG10 wild-type and PG10 Δ*flgM* strains. The number of transformants per microgram of DNA was calculated from three biological replicates (*P* < 0.01, two-tailed paired *t* test). (C) Cell pellets of the PG10 wild type and *flgM* deletion strain.

be similar to those of *B. subtilis* wild-type cells (1). The well-considered design of the blueprint of a mini*Bacillus* cell and extensive laboratory efforts finally led to the construction of the mini*Bacillus* PG10 strain in which 2,700 out of 4,253 genes had been retained (1). Remarkably, despite the immense genome reduction of ~36%, the growth rate of PG10 was only slightly reduced compared to that of its reference strain. Although PG10 cells maintained a rod-shaped morphology, a defect in separation of daughter cells was noted, as cells were observed to form long filaments of unseparated cells. Since this extreme phenotype of PG10 suggests that some level of deregulation in cell division/separation was introduced during the genome reduction process, we sought to investigate the underlying cause(s). We reasoned that identification and elimination of the causes of the cell separation defect of PG10 might lead to an improved mini*Bacillus* strain that is more similar to its parental strain, Δ6. In addition, this might reveal novel targets for subsequent genome minimization steps in this biotechnologically interesting strain.

In this work, genetic and transcriptomic analyses indicated downregulation of autolysins, particularly the major autolysin LytF, to be responsible for the cell separation defect in PG10. This finding agrees with the prominent role of autolysins in the cleavage of peptidoglycan following cell division (5, 6). Inhibition of the SigD regulon, containing *lytABC* and *lytF*, was identified as an underlying factor for the cell separation defect in PG10 (Fig. 6). The activity of SigD was found to be permanently inhibited by intracellular accumulation of its anti-sigma factor, FlgM, due to the absence of the flagellar export apparatus required for secretion of FlgM. The latter appeared to be a

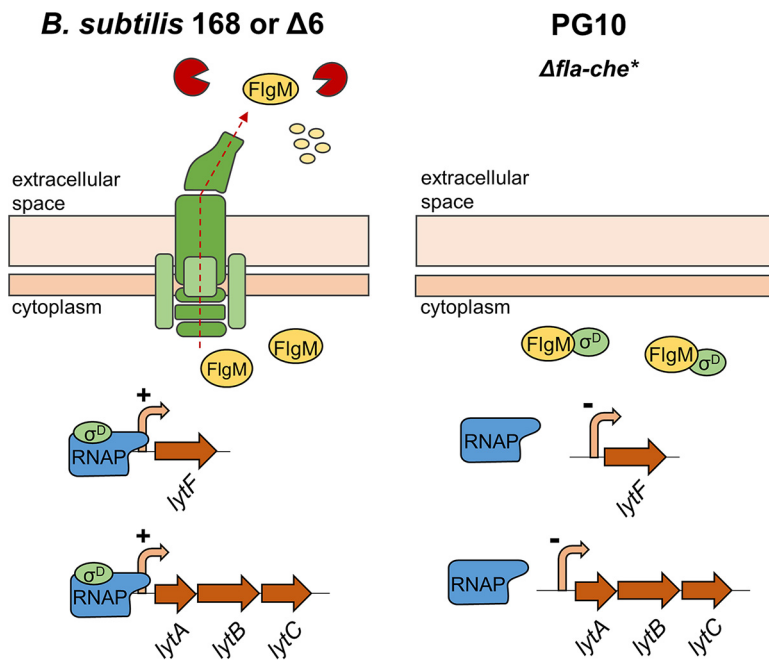


FIG 6 Schematic illustration of underlying causes for the defect in cell separation in PG10. Due to deletion of the majority of genes of the *fla-che* operon (*, *flgB*, *flgC*, *sigD*, and *swrB* are still present), PG10 does not have a flagellar secretion apparatus anymore. This leads to the intracellular accumulation of FlgM, the anti-sigma factor of SigD, causing permanent repression of *lytF* and *lytABC*, resulting in incomplete cell division. For comparison, the normal situation in *B. subtilis* 168 or $\Delta 6$ is shown in which FlgM is secreted after formation of the flagellar secretion apparatus and subsequently degraded by extracellular proteases.

consequence of deletion of the majority of genes of the *fla-che* operon encoding the components of the flagellar export apparatus. The choice to delete these genes was a logical decision, since motility and chemotaxis are not required for growth in complex medium. However, the absence of the flagellar export apparatus indirectly introduced deregulation of the SigD regulon in the resulting minimal cell, with incomplete cell division as a major visible consequence. Out of the 123 genes of the SigD regulon in *B. subtilis* (24), 52 genes are still present in PG10, 23 genes of which are exclusively dependent on SigD for their transcription. Although several genes of the remaining SigD regulon in PG10 are uncharacterized, most genes play a role in motility or chemotaxis, functions of which the majority of genes have been deleted during genome minimization. Therefore, no additional negative effects other than the cell separation defect are expected to have derived from repression of the SigD regulon in PG10. The remaining SigD-regulated genes might be targets for further streamlining of the mini*Bacillus* genome.

As mentioned previously, the cell separation defect of PG10 was not caused by *SlrR*, which, at high expression levels, forms a complex with *SinR* and thereby represses autolysin genes (20). Although sense transcription of *slrR* was unaffected in PG10, the number of antisense transcripts was about 8-fold increased. The latter is a consequence of the fact that *slrR* initially was deleted during the genome reduction process but later on was reintroduced in the *bslA* locus. Along with *bslA*, the terminator of *gbsR* upstream of *bslA* was removed. Since *slrR* was inserted in the inverse orientation in the *bslA* locus, the absence of the *gbsR* terminator caused readthrough from the *gbsR* promoter, thereby producing *slrR* antisense transcripts. Since antisense transcription generally interferes with the expression of the respective gene (25), *slrR* likely became silenced in PG10. In accordance with this, an *slrR* mutant strain displayed the same extensive cell chaining phenotype as the PG10 wild type. This finding also suggests that *slrR* can be permanently deleted from the

genome of PG10 if no adverse effects are observed. Future genome engineering efforts should clarify this.

In addition to understanding the cell separation defect of PG10 as well as identifying new genome reduction targets, we showed that the *flgM* deletion strain displays an increased transformation efficiency of almost 1 order of magnitude. In PG10, genetic competence is artificially initiated by inducing the expression of the master transcriptional regulator of competence, ComK (26). This system was introduced in one of the progenitor strains of PG10, since a gradual decrease in transformability was encountered during the genome reduction process (1). Due to the artificial induction of the competence machinery in PG10, it seems unlikely that an upregulated (uncharacterized) gene of the SigD regulon in the *flgM* deletion strain affected the expression of competence genes and thereby impacted the transformation efficiency. In *B. subtilis*, proteins involved in DNA binding and DNA uptake proteins preferentially localize at the cell poles (27). Therefore, the increased transformation efficiency of the *flgM* deletion strain rather seems to be a consequence of reduced cell chaining. By promoting growth of PG10 as separate cells, cell poles likely become more accessible for competence proteins, thereby facilitating DNA internalization and increasing transformability of PG10. Thus, unchaining PG10 leads to an interesting side effect that facilitates genome engineering in PG10. Preservation of genetic competence is crucial to enable subsequent genome minimization steps.

Although we identified the underlying reasons for the cell separation defect in PG10 and found several beneficial consequences of unchaining PG10, further efforts will be necessary to solve this problem without compromising the fitness of PG10. As indicated previously, deletion of *flgM* could unchain PG10, but aberrant extrusions at the cell poles, a decrease in growth rate, and clumping of cells was observed. An alternative approach for unchaining PG10 might involve reintroduction of the *fla-che* genes necessary for secretion of FlgM. However, this would require a minimum of nine genes of the flagellar export apparatus (14), thereby increasing the genome size of PG10. In addition, it will be unclear whether the extracellular presence of FlgM will have any side effects, since PG10 lacks the extracellular proteases (Epr and WprA) that normally degrade FlgM after its secretion (14). Another possibility would be to knock down *flgM* and analyze whether fine-tuning its expression level prevents the negative consequences that were observed in the case of full deletion of *flgM*. Critically, a proper balance has to be found between the accumulation of FlgM inside the cells and processes contributing to a decrease in its intracellular level (protein instability and dilution of FlgM molecules during cell division). Low constitutive expression of *lytF* also might be a suitable alternative for unchaining PG10, by which adverse effects could be limited.

In conclusion, our work identified the underlying reasons responsible for the cell separation defect in mini*Bacillus* PG10 and provides valuable clues for further optimization of PG10 as a minimal production host.

MATERIALS AND METHODS

Strains and growth conditions. Bacterial strains and plasmids used in this study are listed in Table 3. *B. subtilis* strains were cultured at 37°C with aeration (220 rpm) in LB-Lennox medium (Formedium). *Escherichia coli* (Top10) was used as a cloning host and was grown in LB at 37°C, 220 rpm. For solid medium, growth medium was supplemented with agar (1.5%). When required, LB agar plates for growth of mini*Bacillus* PG10 strains were supplemented with antibiotics at 100 µg/ml spectinomycin or 7 µg/ml kanamycin, whereas half those concentrations were used in liquid cultures. For *E. coli*, 100 µg/ml ampicillin or 30 µg/ml kanamycin was used.

Construction of plasmids and strains. Oligonucleotides used for cloning of plasmids can be found in Table 4 and were synthesized by Biolegio (Nijmegen, the Netherlands). Phusion-HF DNA polymerase, Fast Digest restriction enzymes, and T4 DNA ligase were purchased from Thermo Fisher Scientific. PfuX7 DNA polymerase (purified in our laboratory) was used for colony PCR. Plasmids were constructed by using standard restriction-ligation procedures. All constructs were verified by sequencing. To induce genetic competence in mini*Bacillus* PG10, 0.5% (wt/vol) mannitol was added to the growth medium during exponential phase (26).

pDR-lytF was constructed by prolonged overlap extension (POE) PCR for direct transformation of *B. subtilis* as described previously (28). By regular PCR, *lytF* was amplified with primer pair lytF-fw + lytF-rv from the genomic DNA of PG10, whereas the pDR111 vector was linearized by using primer pair

TABLE 3 List of plasmids and bacterial strains used in this study

Plasmid or strain	Relevant characteristic(s)	Reference or source
Plasmid		
pJOE8999	Vector for markerless genetic engineering of <i>B. subtilis</i> by employing CRISPR-Cas9; Km ^r	30
pJOE_Δ <i>flgM</i>	pJOE8999 derivative for deletion of <i>flgM</i> in PG10	This study
pJOE_Δ <i>slrR</i>	pJOE8999 derivative for deletion of <i>slrR</i> in PG10	This study
pDR111	Integration vector for genomic integration in the <i>amyE</i> locus; carrying an IPTG-inducible promoter (<i>P_{spank-hy}</i>) and <i>lacI</i> ; <i>Spc^r</i>	Laboratory stock
pDR-lytF	pDR111 derivative for the IPTG-inducible expression of the major autolysin <i>lytF</i> ; pDR- <i>P_{spank-hy}</i> -lytF	This study
Strain		
<i>B. subtilis</i>		
168	<i>trp</i> mutant	Laboratory collection
Δ6	Intermediate genome-minimized strain derived from <i>B. subtilis</i> 168 (8% genome reduction)	2
PG10	Large-scale genome-minimized strain derived from <i>B. subtilis</i> 168 (36% genome reduction)	1
PG10 <i>lytF</i>	PG10 derivative; <i>amyE::P_{spank-hy}</i> - <i>lytF</i>	This study
PG10 Δ <i>flgM</i>	PG10 derivative; Δ <i>flgM</i>	This study
PG10 Δ <i>slrR</i>	PG10 derivative; Δ <i>slrR</i>	This study
<i>E. coli</i> Top10	F- <i>mcrA</i> Δ(<i>mrr</i> - <i>hsdRMS</i> - <i>mcrBC</i>) Φ80 <i>lacZ</i> Δ <i>M15</i> Δ <i>lacX74</i> <i>recA1</i> <i>araD139</i> Δ(<i>ara leu</i>)7697 <i>galU</i> <i>galK</i> <i>rpsL</i> (<i>strR</i>) <i>endA1</i> <i>nupG</i>	Laboratory collection

pDR111-fw + pDR111-rv. In both PCR products, 5' and 3' overlapping termini of about 25 bp were introduced. Next, POE-PCR was performed as described previously (29), and resulting multimers were used for direct transformation of PG10.

For the markerless deletion of *slrR* or *flgM* in PG10, two pJOE8999 vectors were constructed. A specific single guide RNA (sgRNA)-encoding sequence was designed using the CRISPR Guide Design Software of Benchling (*slrR*, ATGATGTATGAAAAATCAG; *flgM*, AAAAAATTATGATAAGCAAG) and cloned into pJOE8999 via Eco31I digestion. To enable homologous recombination, up- and downstream flanking regions to construct pJOE_Δ*slrR* and pJOE_Δ*flgM* were obtained from the genomic DNA of *B. subtilis* 168. For pJOE_Δ*slrR*, primer pairs *slrR*-up-fw + *slrR*-up-rv (up) and *slrR*-down-fw + *slrR*-down-rv (down) were used. To obtain the final pJOE_Δ*slrR* vector, flanking regions were digested with SfiI followed by ligation into similarly digested pJOE vector with the sgRNA-encoding sequence. For flanking regions of *flgM*, primer pairs *flgM*-up-fw + *flgM*-up-rv (up) and *flgM*-down-fw + *flgM*-down-rv (down) were used. pJOE8999 containing the *flgM* guide was linearized by PCR using primer pair pJOE-fw + pJOE-rv. Eco31I digestion of *flgM* flanking regions and pJOE backbone followed by T4-ligation yielded pJOE_Δ*flgM*.

Microscopy. For microscopic analysis, 1 μl of culture was pipetted on a thin layer of 1.5% (wt/vol) agarose on a microscope slide and air dried. Phase-contrast images were taken on a DeltaVision Elite inverted microscope (Applied Precision, GE Healthcare) equipped with an sCMOS camera, using a 100× oil, 1.4-numeric-aperture objective. Digital images were acquired with SoftWorX 3.6.0 software (Applied Precision) and analyzed using ImageJ Fiji.

Transcriptome analysis. Whole-genome tiling array data derived from the initial characterization of PG10 (1) was retrieved from the Gene Expression Omnibus (GEO) database under accession number

TABLE 4 List of oligonucleotides used in this study

Primer	Nucleotide sequence (5'–3')
lytF-fw	CGGTGCAAAACGATATTTCTAAAAACCATTAGCATCACCTTGCTC
lytF-rv	CCTGCTGCTAATTTCTTTTTCATATTGGTCACCTCCTTTC
pDR111-fw	GCTTATTGAAAGGAGGTGACCAATATGAAAAAGAAATTAGCAGCAGG
pDR111-rv	GAGCAAGGTGATGCTAATGGTTTTAGAAATATCGTTTTGCACCCG
<i>flgM</i> -up-fw	TCGAGGTCTCAAAGACACTAGAAATTGACACAGGC
<i>flgM</i> -up-rv	TCGAGGTCTCAATCCCTTTTATCGACTGCGTTTTTC
<i>flgM</i> -down-fw	TCGAGGTCTCAGGATAAGGAGAAAGCCCATGTCAG
<i>flgM</i> -down-rv	TCGAGGTCTCACAGCCGGCAGCTCAGCTTAAATTG
<i>slrR</i> -up-fw	CGTAGGCCAACGCGCCGGATGAATAATGCGGTCAGC
<i>slrR</i> -up-rv	CGTAGGCCGAAGTGGCCGCTGTTATTTCTGTTCAATTATAAG
<i>slrR</i> -down-fw	GCTAGGCCAGTTCGGCCCTGTCATGAAGTCAAATCC
<i>slrR</i> -down-rv	CGTAGGCCGATTGGCCCTGATAATACTGCGGATCTG
pJOE-fw	TCGAGGTCTCATCTTTGGCCGTCGACCCTATAGTG
pJOE-rv	TCGAGGTCTCAGCTGGCCCTTTCTAGATTAAGAAATA

GSE82249. Differentially expressed genes were determined using the GEO2R web tool (adjusted P value of ≤ 0.05). The average of the sense/antisense reads of *slrR* was determined by calculating the average of the fragments overlapping with the gene from all four replicates of PG10 and $\Delta 6$ (1).

Growth measurements. To generate growth curves of the different PG10 strains, *B. subtilis* $\Delta 6$ and *B. subtilis* 168, three biological replicates of each strain were cultured in 10 ml of LB starting at an OD_{600} of 0.05. During growth at 37°C and 220 rpm, the OD_{600} was measured every hour after thoroughly pipetting the cell suspension to dissolve cellular aggregates. Average values and standard deviations were calculated from the triplicate measurements. A two-tailed paired t test was used to statistically compare the growth between PG10 wild-type and PG10 mutant strains ($P < 0.05$).

Determination of transformation efficiency. To determine the transformation efficiency of PG10 strains, three biological replicates were used. Competence was induced by addition of 0.5% (wt/vol) mannitol to the growth medium at an OD_{600} of 0.2. After ~ 1.5 h, growth cultures of different strains were diluted to the same OD_{600} (0.4), and 100 ng of plasmid DNA was added to 1 ml of cell suspension. After 1 h of incubation at 37°C and 220 rpm, the cell suspension was plated in serial dilutions and incubated at 37°C. The next day, the number of colonies was counted and corrected per microgram of DNA. Average values and standard deviations were calculated. Statistical analysis was performed using a two-tailed paired t test ($P < 0.01$).

SUPPLEMENTAL MATERIAL

Supplemental material is available online only.

SUPPLEMENTAL FILE 1, PDF file, 0.2 MB.

ACKNOWLEDGMENTS

A.Y.V.T. and A.J.V.H. were supported by a grant from the European Union's Horizon 2020 research and innovation program (grant agreement no. 720776).

A.Y.V.T., A.J.V.H., and O.P.K. conceived the study. O.P.K., J.S., and U.V. secured funding of the project and guided the project. A.Y.V.T. designed, performed, and analyzed experiments, wrote the manuscript, and prepared figures. J.A.F. designed, performed, and analyzed experiments. A.R. carried out specific experiments. A.J.V.H. contributed to the design of the experiments, data analysis, and interpretation of the results. All authors contributed to correction of the manuscript.

REFERENCES

1. Reuß DR, Altenbuchner J, Mäder U, Rath H, Ischebeck T, Sappa PK, Thürmer A, Guérin C, Nicolas P, Steil L, Zhu B, Feussner I, Klumpp S, Daniel R, Commichau FM, Völker U, Stülke J. 2017. Large-scale reduction of the *Bacillus subtilis* genome: consequences for the transcriptional network, resource allocation, and metabolism. *Genome Res* 27:289–299. <https://doi.org/10.1101/gr.251293.116>.
2. Westers H, Dorenbos R, Van Dijk JM, Kabel J, Flanagan T, Devine KM, Jude F, Séror SJ, Beekman AC, Darmon E, Eschevins C, De Jong A, Bron S, Kuipers OP, Albertini AM, Antelmann H, Hecker M, Zamboni N, Sauer U, Bruand C, Ehrlich DS, Alonso JC, Salas M, Quax WJ. 2003. Genome engineering reveals large dispensable regions in *Bacillus subtilis*. *Mol Biol Evol* 20:2076–2090. <https://doi.org/10.1093/molbev/msg219>.
3. Aguilar Suárez R, Stülke J, Van Dijk JM. 2019. Less is more: toward a genome-reduced *Bacillus* cell factory for "difficult proteins." *ACS Synth Biol* 8:99–108. <https://doi.org/10.1021/acssynbio.8b00342>.
4. van Tilburg AY, van Heel AJ, Stülke J, de Kok NAW, Rueff AS, Kuipers OP. 2020. Mini*Bacillus* PG10 as a convenient and effective production host for lantibiotics. *ACS Synth Biol* 9:1833–1842. <https://doi.org/10.1021/acssynbio.0c00194>.
5. Smith TJ, Blackman SA, Foster SJ. 2000. Autolysins of *Bacillus subtilis*: multiple enzymes with multiple functions. *Microbiology* 146:249–262. <https://doi.org/10.1099/00221287-146-2-249>.
6. Chen R, Guttenplan SB, Blair KM, Kearns DB. 2009. Role of the SigD-dependent autolysins in *Bacillus subtilis* population heterogeneity. *J Bacteriol* 191:5775–5784. <https://doi.org/10.1128/JB.00521-09>.
7. Kearns DB, Losick R. 2005. Cell population heterogeneity during growth of *Bacillus subtilis*. *Genes Dev* 19:3083–3094. <https://doi.org/10.1101/gad.1373905>.
8. Branda SS, González-Pastor JE, Ben-Yehuda S, Losick R, Kolter R. 2001. Fruiting body formation by *Bacillus subtilis*. *Proc Natl Acad Sci U S A* 98:11621–11626. <https://doi.org/10.1073/pnas.191384198>.
9. Helmann JD, Márquez LM, Chamberlin MJ. 1988. Cloning, sequencing, and disruption of the *Bacillus subtilis* *sigma 28* gene. *J Bacteriol* 170:1568–1574. <https://doi.org/10.1128/jb.170.4.1568-1574.1988>.
10. Mirel DB, Chamberlin MJ. 1989. The *Bacillus subtilis* flagellin gene (*hag*) is transcribed by the sigma 28 form of RNA polymerase. *J Bacteriol* 171:3095–3101. <https://doi.org/10.1128/jb.171.6.3095-3101.1989>.
11. Márquez LM, Helmann JD, Ferrari E, Parker HM, Ordal GW, Chamberlin MJ. 1990. Studies of sigma D-dependent functions in *Bacillus subtilis*. *J Bacteriol* 172:3435–3443. <https://doi.org/10.1128/jb.172.6.3435-3443.1990>.
12. Kuroda A, Sekiguchi J. 1993. High-level transcription of the major *Bacillus subtilis* autolysin operon depends on expression of the *sigma D* gene and is affected by a *sin (flaD)* mutation. *J Bacteriol* 175:795–801. <https://doi.org/10.1128/jb.175.3.795-801.1993>.
13. Margot P, Pagni M, Karamata D. 1999. *Bacillus subtilis* 168 gene *lytF* encodes a gamma-D-glutamate-meso-diaminopimelate muropeptidase expressed by the alternative vegetative sigma factor, sigmaD. *Microbiology* 145:57–65. <https://doi.org/10.1099/13500872-145-1-57>.
14. Calvo RA, Kearns DB. 2015. FlgM is secreted by the flagellar export apparatus in *Bacillus subtilis*. *J Bacteriol* 197:81–91. <https://doi.org/10.1128/JB.02324-14>.
15. Marquez-Magana LM, Chamberlin MJ. 1994. Characterization of the *sigD* transcription unit of *Bacillus subtilis*. *J Bacteriol* 176:2427–2434. <https://doi.org/10.1128/jb.176.8.2427-2434.1994>.
16. Albertini AM, Caramori T, Crabb WD, Scoffone F, Galizzi A. 1991. The *flaA* locus of *Bacillus subtilis* is part of a large operon coding for flagellar structures, motility functions, and an ATPase-like polypeptide. *J Bacteriol* 173:3573–3579. <https://doi.org/10.1128/jb.173.11.3573-3579.1991>.
17. Mirel DB, Lauer P, Chamberlin MJ. 1994. Identification of flagellar synthesis regulatory and structural genes in a sigma D-dependent operon of *Bacillus subtilis*. *J Bacteriol* 176:4492–4500. <https://doi.org/10.1128/jb.176.15.4492-4500.1994>.

18. Caramori T, Barilla D, Nessi C, Sacchi L, Galizzi A. 1996. Role of FlgM in SigD-dependent gene expression in *Bacillus subtilis*. *J Bacteriol* 178:3113–3118. <https://doi.org/10.1128/jb.178.11.3113-3118.1996>.
19. Bertero MG, Gonzales B, Tarricone C, Cecilian F, Galizzi A. 1999. Overproduction and characterization of the *Bacillus subtilis* anti-sigma factor FlgM. *J Biol Chem* 274:12103–12107. <https://doi.org/10.1074/jbc.274.17.12103>.
20. Chai Y, Norman T, Kolter R, Losick R. 2010. An epigenetic switch governing daughter cell separation in *Bacillus subtilis*. *Genes Dev* 24:754–765. <https://doi.org/10.1101/gad.1915010>.
21. Bai U, Mandic-Mulec I, Smith I. 1993. SinI modulates the activity of SinR, a developmental switch protein of *Bacillus subtilis*, by protein-protein interaction. *Genes Dev* 7:139–148. <https://doi.org/10.1101/gad.7.1.139>.
22. Ohnishi R, Ishikawa S, Sekiguchi J. 1999. Peptidoglycan hydrolase LytF plays a role in cell separation with CwF during vegetative growth of *Bacillus subtilis*. *J Bacteriol* 181:3178–3184. <https://doi.org/10.1128/JB.181.10.3178-3184.1999>.
23. Reuß DR, Commichau FM, Gundlach J, Zhu B, Stülke J. 2016. The blueprint of a minimal cell: mini*Bacillus*. *Microbiol Mol Biol Rev* 80:955–987. <https://doi.org/10.1128/MMBR.00029-16>.
24. Zhu B, Stülke J. 2018. SubtiWiki in 2018: from genes and proteins to functional network annotation of the model organism *Bacillus subtilis*. *Nucleic Acids Res* 46:D743–D748. <https://doi.org/10.1093/nar/gkx908>.
25. Georg J, Hess WR. 2018. Widespread antisense transcription in prokaryotes. *Microbiol Spectr* <https://doi.org/10.1128/microbiolspec.RWR-0029-2018>.
26. Rahmer R, Heravi KM, Altenbuchner J. 2015. Construction of a super-competent *Bacillus subtilis* 168 using the *PmtIA-comKS* inducible cassette. *Front Microbiol* 6:1431. <https://doi.org/10.3389/fmicb.2015.01431>.
27. Hahn J, Maier B, Hajjema BJ, Sheetz M, Dubnau D. 2005. Transformation proteins and DNA uptake localize to the cell poles in *Bacillus subtilis*. *Cell* 122:59–71. <https://doi.org/10.1016/j.cell.2005.04.035>.
28. You C, Zhang XZ, Zhang YHP. 2012. Simple cloning via direct transformation of PCR product (DNA multimer) to *Escherichia coli* and *Bacillus subtilis*. *Appl Environ Microbiol* 78:1593–1595. <https://doi.org/10.1128/AEM.07105-11>.
29. Zhong C, You C, Wei P, Zhang Y-HP. 2017. Simple cloning by prolonged overlap extension-PCR with application to the preparation of large-size random gene mutagenesis library in *Escherichia coli*. *Methods Mol Biol* 1472:49–61. https://doi.org/10.1007/978-1-4939-6343-0_4.
30. Altenbuchner J. 2016. Editing of the *Bacillus subtilis* genome by the CRISPR-Cas9 system. *Appl Environ Microbiol* 82:5421–5427. <https://doi.org/10.1128/AEM.01453-16>.

